Short communication

Li$_{1.2}$Zr$_{1.9}$Ca$_{0.1}$(PO$_4$)$_3$, a room-temperature Li-ion solid electrolyte

Hui Xie [a], John B. Goodenough [a,*], Yutao Li [b]

[a] *Texas Materials Institute, ETC 9.184, University of Texas at Austin, Austin, TX 78712, United States*
[b] *State Key Laboratory of New Ceramics and Fine Processing, Department of Materials Science and Engineering, Tsinghua University, Beijing 100084, PR China*

ARTICLE INFO

ABSTRACT

Substitution of 5% of Zr by Ca in LiZr$_2$(PO$_4$)$_3$ transforms the structure to that of rhombohedral NASICON to give a room-temperature bulk Li-ion conductivity $\sigma_{Li} \approx 1.2 \times 10^{-4}$ S cm^{-1}, which is comparable to that of Li$_{1.3}$Ti$_{1.7}$Al$_{0.3}$(PO$_4$)$_3$ now being used as a solid Li-ion separator in test cells of novel Li-ion batteries.

© 2011 Elsevier B.V. All rights reserved.

1. Introduction

Interest in all-solid-state Li-ion batteries and in Li-ion batteries using a solid separator of an organic-liquid electrolyte on the anode side and an aqueous or air cathode has stimulated the search for Li-ion solid electrolytes having a room-temperature Li-ion conductivity $\sigma_{Li} > 10^{-4}$ S cm^{-1} [1,2]. Although sulfides promise a higher σ_{Li} than oxides, they cannot be used if there is an aqueous solution on the cathode side of a solid separator. At present, the best commercially available oxide Li-ion solid electrolyte is slightly-modified Li$_{1.3}$Ti$_{1.7}$Al$_{0.3}$(PO$_4$)$_3$ [3–5] having the structure of rhombohedral NASICON [6,7]. However, the presence of the Ti(IV) ion makes it necessary for an aqueous cathode solution to be restricted to a limited pH range. Therefore, there is motivation to find an isostructural oxide of comparable σ_{Li} that does not contain a cation so easily reduced as Ti(IV).

The zirconium phosphate LiZr$_2$(PO$_4$)$_3$ can be expected to be electrochemically more stable than the LiTi$_2$(PO$_4$)$_3$ analog since Zr(IV) is a stable oxidation state in oxides containing isolated (ZrO$_6$) octahedra. However, LiZr$_2$(PO$_4$)$_3$ is triclinic at room temperature with a $\sigma_{Li} \approx 10^{-8}$ S cm^{-1} [8,9], the rhombohedra NASICON structure of LiZr$_2$(PO$_4$)$_3$, which is the structure allowing fast alkali-ion transport, is only stable above 50 °C [10]. Since a higher σ_{Li} can be attained by aliovalent doping of LiTi$_2$(PO$_4$)$_3$ to introduce mobile Li$^+$ ions in the M(II) site of the interstitial space [11], we have investigated doping LiZr$_2$(PO$_4$)$_3$ by substitution of Ca for Zr, thereby introducing additional Li$^+$ ions and favoring stabilization to room temperature of the rhombohedral phase.
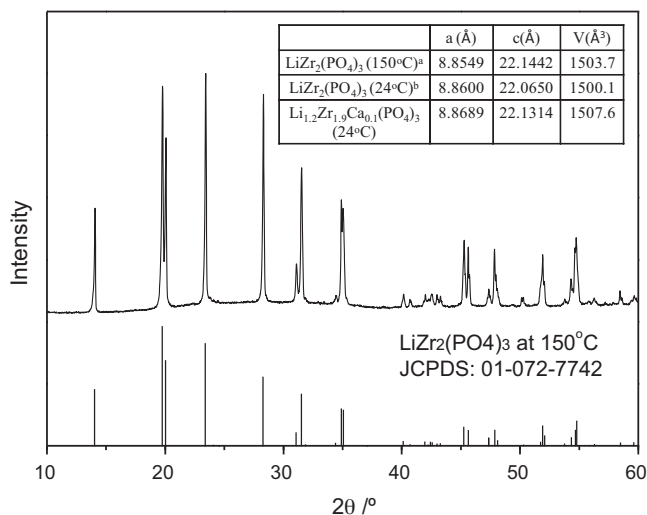
2. Experimental

The compound Li$_{1.2}$Zr$_{1.9}$Ca$_{0.1}$(PO$_4$)$_3$ was prepared by conventional solid state reaction as described in Ref. [8] with Li$_2$CO$_3$, ZrO$_2$, NH$_4$H$_2$PO$_4$, CaCO$_3$ as the starting materials. 10% more Li$_2$CO$_3$ was used to compensate for the loss of lithium during the high temperature heating processes. A pellet of high mechanical strength was obtained after the final heat treatment.

Powder X-ray diffractogram (Philips X-ray diffractometer, model: PW 1830) recorded in air at room temperature was applied to investigate the phase formation and to calculate the lattice parameters. The scanning range was from 10° to 60°, with a step of 0.02° and a dwell time of 12 s. Rietveld structure refinement was carried out with the FullProf software.

Field-emission scanning electron microscopy (FESEM, Quanta FEG 650) with an EDS attachment (Bruker) was used to obtain the surface microstructure of the pellet and the distribution of the zirconium and calcium elements.

To measure the ionic conductivity, both parallel surfaces of the pellet were sputtered with a layer of gold. The ionic conductivity was obtained from the impedance plot measured with a Solartron Impedance Analyzer (model 1287). The applied frequency range was from 10^6 to 1 Hz with a 10 mV AC amplitude. The Li-ion conduction activation energy (E_a) was calculated from the Arrhenius plot of the relationship of the total ionic conductivity to temperature.

---

* Corresponding author. Tel.: +1 512 471 1646; fax: +1 512 471 7681.
E-mail address: jgoodenough@mail.utexas.edu (J.B. Goodenough).

a Obtained from neutron diffraction recorded at 150°C from ref. 10.

b Extropolated to room temperature from the thermal expansion data obtained from ref. 10.

Fig. 1. Measured powder XRD pattern of $Li_{1.2}Zr_{1.9}Ca_{0.1}(PO_4)_3$ compared with standard $LiZr_2(PO_4)_3$ at 150°C (JCPDS#: 01-072-7742) reported in Joint Committee on Powder Diffraction Standards. Inset table lists the lattice parameters obtained from the two patterns with that extrapolated to room temperature from the thermal-expansion data.

Fig. 3. (a) Impedance plot collected at room temperature (about 24°C) in air with the fitted curve and (b) the equivalent circuit applied to fit the impedance plot.

3. Results and discussions

The XRD pattern of the compound after sintering is shown in Fig. 1. It is clear that the obtained compound can be indexed to the rhombohedral NASICON structure. No impurity peak was observed. In the inset, we compare the lattice parameters of the obtained compound with those of the pure $LiZr_2(PO_4)_3$ with the same structure (JCPSD#: 01-072-7742) obtained at 150°C [10]. Structural data extrapolated to room temperature from the thermal-expansion data above 150°C are also listed in the table. It is shown that both a and c dimensions increase on doping with Ca^{2+}; the Ca^{2+} ion is significantly larger than Zr^{4+}. The DTA curve (not shown in the paper) obtained in flowing air atmosphere from room temperature to 1000°C shows no detectable endothermic or exothermic peak on both heating and cooling, which indicates that the NASICON phase is thermally stable to at least 1000°C.
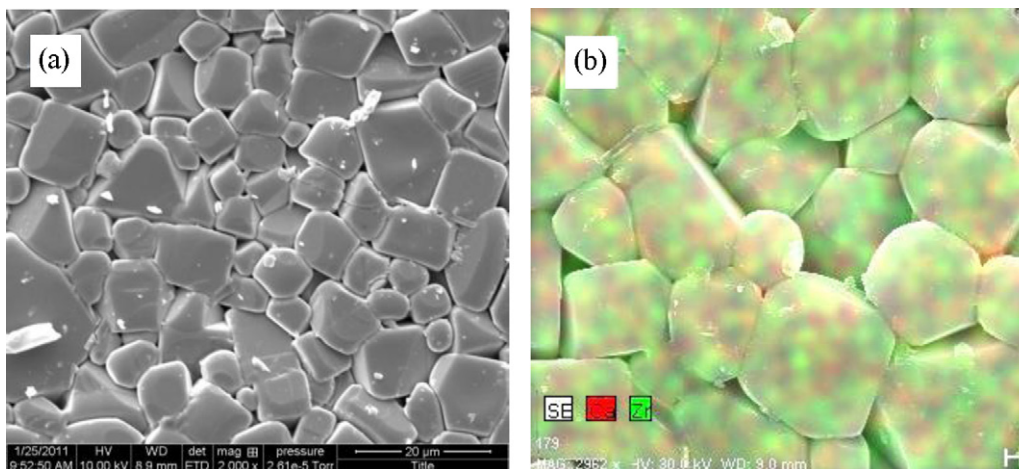
Fig. 2a displays the surface microstructure of the pellet after sintering. The grains are in good contact with each other although a certain amount of pores in the boundary area can be observed. Most of the particles are 5–10 μm in size. The distribution of Zr and Ca elements obtained by EDS is shown in Fig. 2b. The Zr and Ca elements are seen to be evenly distributed throughout the whole area.

The impedance plot and its fitted curve (solid line) at room temperature are presented in Fig. 3a with the equivalent circuit in Fig. 3b [12,13]. In the circuit, R is for resistance, Q for constant phase element. R_e is added to the circuit due to the electronic resistance of the measurement system; subscripts b and g refer to bulk and grain boundary, respectively, and el is the blocking electrode, which corresponds to the long tail at the low frequency end of the plot. This long tail indicates that the material is an ionic conductor [13]. The impedance plot consists of two semicircles at high temperature range, as is clearly shown in the inset of Fig. 3a. The first

Fig. 2. (a) The surface microstructure of the sintered pellet; (b) the mapping image of the elemental analysis obtained by EDS of zirconium (green) and calcium element (red). (For interpretation of the references to color in this figure caption, the reader is referred to the web version of the article.)
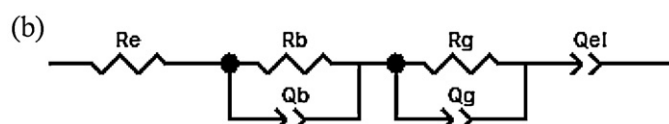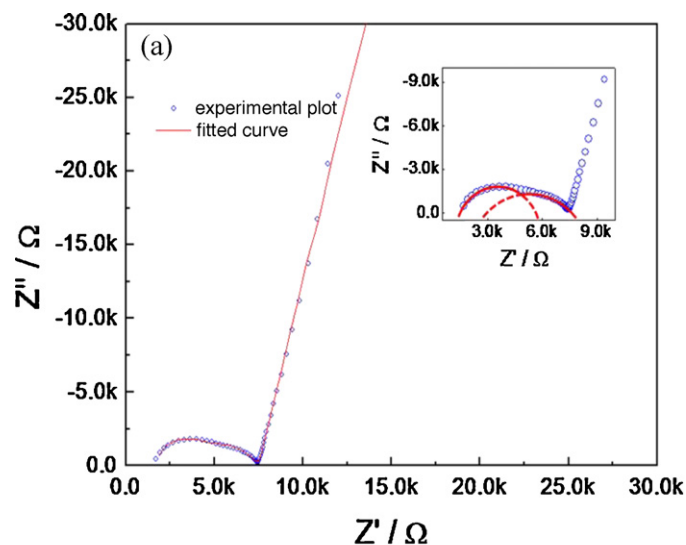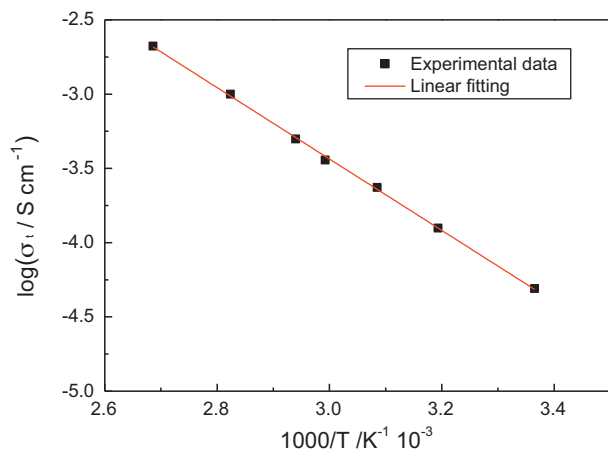
Fig. 4. Arrhenius plot of the total ionic conductivity.

semicircle at the high frequency end is ascribed to the bulk and that at the intermediate frequency range to the grain boundary.

The bulk ionic conductivity calculated from the fitted result is 1.2×10^{-4} S cm^{-1}. However, due to the porous structure of the sintered pellet as shown in Fig. 2a, the grain-boundary resistance is higher than the bulk. In fact, the grain boundary contributes about 59% of the total resistance of the sample. Consequently, the total ionic conductivity is about 0.49×10^{-4} S cm^{-1}, still several times higher than that of pure $LiZr_2(PO_4)_3$ with the NASICON structure at about 50 °C [10].

The activation energy E_a for the Li-ion conduction of the material can be obtained from the Arrhenius plot of $\sigma = \sigma_0 \exp(-E_a/kT)$, where σ_0 is the pre-exponential factor, R is the universal gas constant, k is the Boltzmann constant, T is the absolute temperature.

Since it is difficult to separate the bulk and grain-boundary contributions at temperatures above room temperature with the impedance spectra, the total ionic conductivity was determined. The Arrhenius plot shown in Fig. 4 gives an $E_a = 0.48$ eV.

Although the total ionic conductivity is lower than that required for practical application at room temperature, these properties may be further improved through optimizing the doping element and content [14,15] by: (a) increasing the density of the bulk material to minimize the grain-boundary resistance; (b) introducing more Li into the framework to increase the mobile-ion concentration and (c) tuning the lattice parameter to optimize the size of the interstitial channel for Li-ion conduction.

4. Conclusion

The introduction of Ca into $LiZr_2(PO_4)_3$ stabilizes the rhombohedral NASICON structure and increases the Li-ion concentration to give a dramatic increase in the bulk Li-ion conductivity to $\sigma_{Li} \approx 1.2 \times 10^{-4}$ S cm^{-1}. A measured activation energy $E_a = 0.48$ eV includes the grain-boundary contribution that can be decreased by densification of the solid. The octahedral-site Zr(IV) should not be reduced in any anticipated applications. Based on the fact that the ionic conductivity of the pure $LiZr_2(PO_4)_3$ with the NASICON structure is higher than that of the $LiTi_2(PO_4)_3$ with the same structure, we believe that $LiZr_2(PO_4)_3$ is a promising host material for fast Li-ion conduction.

Acknowledgements

References

[1] V. Thangadurai, A.K. Shukla, J. Gopalakrishnan, J. Mater. Chem. 9 (1999) 739–741.
[2] A. Ramzy, V. Thangadurai, ACS Appl. Mater. Interfaces 2 (2010) 385–390.
[3] H. Aono, E. Sugimoto, Y. Sadaoka, N. Imanaka, G.Y. Adachi, J. Electrochem. Soc. 136 (1989) 590–591.
[4] H. Aono, E. Sugimoto, Y. Sadaoka, N. Imanaka, G. Adachi, J. Electrochem. Soc. 137 (1990) 1023–1027.
[5] S. Hasegawa, N. Imanishi, T. Zhang, J. Power Sources 189 (2010) 371–377.
[6] J.B. Goodenough, H.Y.-P. Hong, J.A. Kafalas, Mater. Res. Bull. 11 (1976) 203–220.
[7] C.L. Tsai, H.Y.P. Hong, Mater. Res. Bull. 18 (1983) 1399–1407.
[8] M. Catti, S. Stramare, R. Ibberson, Solid State Ionics 123 (1999) 173–180.
[9] K. Arbi, M. Ayadi-Trabelsi, J. Sanz, J. Mater. Chem. 12 (2002) 2985–2990.
[10] M. Catti, A. Comotti, S. Di Blas, Chem. Mater. 15 (2003) 1628–1632.
[11] J.B. Goodenough, Energy, Mine and Resources, Ottawa, Canada, 1983.
[12] E. Barasoukov, J.R. MacDonald, Impedance Spectroscopy, Wiley-interscience, 2005.
[13] R. Murugan, V. Thangadurai, W. Weppner, Angew. Chem. Int. Edit. 46 (2007) 7778–7781.
[14] M. Barre, M.P. Crosnier-Lopez, F. Le Berre, E. Suard, J.L. Fourquet, J. Solid State Chem. 180 (2007) 1011–1019.
[15] I.A. Stenina, M.N. Kislitsyn, I.Y. Pinus, S.M. Haile, A.B. Yaroslavtsev, Diffusion in Solids—Past, Present and Future, vol. 249, 2006, pp. 255–262.